We are IntechOpen, the world's leading publisher of Open Access books
Built by scientists, for scientists

6,900
Open access books available

185,000
International authors and editors

200M
Downloads

Our authors are among the

154
Countries delivered to

TOP 1%
most cited scientists

12.2%
Contributors from top 500 universities

WEB OF SCIENCE™

Selection of our books indexed in the Book Citation Index in Web of Science™ Core Collection (BKCI)

Interested in publishing with us?
Contact book.department@intechopen.com

Numbers displayed above are based on latest data collected.
For more information visit www.intechopen.com

Chapter

Optical Propagation in Magneto-Optical Materials

Licinius Dimitri Sá de Alcantara

Abstract

Magneto-optical materials present anisotropy in the electrical permittivity controlled by a magnetic field, which affects the propagation characteristics of light and stands out in the design of nonreciprocal devices, such as optical isolators and circulators. Based on Maxwell's equations, this chapter focuses on the wave propagation in magneto-optical media. The following cases are covered: The propagation of a plane wave in an unbounded magneto-optical medium, where the phenomenon of Faraday rotation is discussed, and the guided propagation in planar magneto-optical waveguides with three and five layers, highlighting the phenomenon of nonreciprocal phase shift and its potential use on the design of nonreciprocal optical devices.

Keywords: magneto-optical media, light propagation, Faraday rotation, nonreciprocal phase shift, optical devices

1. Introduction

A material is classified as magneto-optical (MO) if it affects the propagation characteristics of light when an external magnetic field is applied on it. For ferromagnetic materials, which are composed by magnetically ordered domains, MO phenomena may also occur in the absence of an external magnetic field. A great number of magneto-optical phenomena are the direct or indirect outcome of the splitting of energy levels in an external or spontaneous magnetic field [1].

The MO effect depends on the polarization of the magnetic field. It also depends on the polarization of the light and on its propagation direction, so it is an anisotropic phenomenon, which has attracted great attention from researchers in optical devices. The MO materials can have their anisotropy controlled by a magnetostatic field (H_{DC}), and this behavior can be exploited on the design of nonreciprocal devices. By nonreciprocal devices or structures, it means that waves or guided modes supported by them have their propagation characteristics altered when the wave propagation sense is reversed. Optical isolators and circulators can be highlighted as examples of such devices. Isolators are designed to protect optical sources from reflected light and are present in optical amplification systems. The circulators are employed as signal routers and act in devices that extract wavelengths in WDM systems.

The design of optical devices with MO materials is addressed in several works such as [2–5]. The challenges for the design of such devices are the development of MO materials with high-induced anisotropy and high transparency at the optical

spectrum. Therefore, research activities on the improvement of MO materials and structures have also great relevance and are covered in works such as [6–10]. Integration of MO materials and structures with other optical system components, with reduction of insertion losses, is also a target for researches in optical devices. Research of MO effects in optical structures such as photonic crystals has also been addressed [11–13].

This chapter presents analytical formalisms derived from Maxwell's and wave equations to analyze the propagation characteristics of transverse electromagnetic (TEM) waves in unbounded magneto-optical material. The guided propagation characteristics of transverse magnetic (TM) modes in three- and five-layered planar magneto-optical waveguides are also formalized and discussed. The analytical formalism is versatile so that each layer can be set as magneto-optical or isotropic in the mathematical model.

2. Wave propagation characteristics

This section focuses on the optical propagation analysis in magneto-optical media using Maxwell's equations as starting point. In a magnetized MO media, cyclotron resonances occur at optical frequencies, if the wave is properly polarized. This physical phenomenon induces a coupling between orthogonal electric field components in the plane perpendicular to the applied magnetostatic field H_{DC}, which affects the wave polarization. Depending on the orientation of the magnetostatic field, the configuration of the electric permittivity tensor changes. If H_{DC} is oriented along one of the Cartesian axes, the relative electric permittivity assumes the form

$$\bar{\bar{\varepsilon}}_r = \begin{bmatrix} n^2 & 0 & 0 \\ 0 & n^2 & j\delta \\ 0 & -j\delta & n^2 \end{bmatrix}, \text{for } H_{DC} \parallel x - \text{axis;} \tag{1}$$

$$\bar{\bar{\varepsilon}}_r = \begin{bmatrix} n^2 & 0 & j\delta \\ 0 & n^2 & 0 \\ -j\delta & 0 & n^2 \end{bmatrix}, \text{for } H_{DC} \parallel y - \text{axis;} \tag{2}$$

$$\bar{\bar{\varepsilon}}_r = \begin{bmatrix} n^2 & j\delta & 0 \\ -j\delta & n^2 & 0 \\ 0 & 0 & n^2 \end{bmatrix}, \text{for } H_{DC} \parallel z - \text{axis.} \tag{3}$$

where n is the refractive index of the material and δ is the magneto-optical constant. The MO constant is proportional to H_{DC}. If the sense of H_{DC} is reversed, $\delta(\text{-}H_{DC}) = -\delta(H_{DC})$, and for $H_{DC} = 0$, the off-diagonal components of the electric permittivity tensor are zero [14, 15].

2.1 TEM wave in an unbounded magneto-optical medium

Let us consider a TM wave propagating in an unbounded MO medium, as shown in **Figure 1**.

From Maxwell's equations, the vectorial Helmholtz equation for anisotropic media and for the electric field $\overline{E}(x,y,z)$ can be written as

$$\omega^2 \mu_0 \varepsilon_0 \bar{\bar{\varepsilon}}_r \overline{E} + \nabla^2 \overline{E} - \nabla\left(\nabla \cdot \overline{E}\right) = \overline{0}, \tag{4}$$

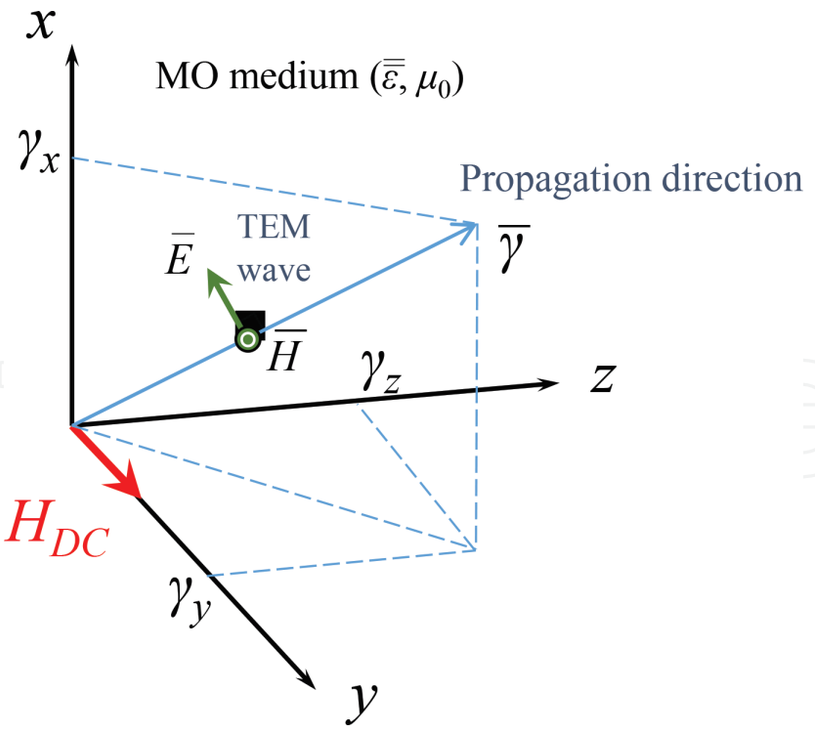

Figure 1.
TEM wave in an unbounded magneto-optical medium.

where ω is the angular frequency in rad/s, μ_0 is the magnetic permeability of the vacuum in H/m, and ε_0 is the electric permittivity of the vacuum in F/m.

To develop a plane wave solution for MO media, it is assumed that H_{DC} is parallel to the y-axis and $\bar{\bar{\varepsilon}}_r$ is given by Eq. (2) from now on. This assumption does not imply on lack of generality because it is assumed that the wave propagates at an arbitrary direction, with the electric field vector given by

$$\bar{E} = \bar{E}_0 \exp(j\omega t) \exp\left[-j\left(\gamma_x x + \gamma_y y + \gamma_z z\right)\right]. \tag{5}$$

where $\bar{\gamma} = \gamma_x \vec{\mathbf{i}} + \gamma_y \vec{\mathbf{j}} + \gamma_z \vec{\mathbf{k}}$ is the propagation constant vector.

From Gauss' law for a medium with equilibrium of charges, $\nabla.\left(\varepsilon_0 \bar{\bar{\varepsilon}}_r \bar{E}\right) = 0$, we obtain:

$$\nabla \cdot \bar{E} = j\frac{\delta}{n^2}\left(\frac{\partial E_x}{\partial z} - \frac{\partial E_z}{\partial x}\right). \tag{6}$$

Substituting Eq. (6) into Eq. (4) leads to

$$\omega^2 \mu_0 \varepsilon_0 \bar{\bar{\varepsilon}}_r \bar{E} + \nabla^2 \bar{E} - j\frac{\delta}{n^2}\nabla\left(\frac{\partial E_x}{\partial z} - \frac{\partial E_z}{\partial x}\right) = \bar{0}. \tag{7}$$

Expanding Eq. (7) in the Cartesian coordinates results in

$$\omega^2 \mu_0 \varepsilon_0 \left(n^2 E_x + j\delta E_z\right) + \frac{\partial^2 E_x}{\partial x^2} + \frac{\partial^2 E_x}{\partial y^2} + \frac{\partial^2 E_x}{\partial z^2} - j\frac{\delta}{n^2}\left(\frac{\partial^2 E_x}{\partial x \partial z} - \frac{\partial^2 E_z}{\partial x^2}\right) = 0, \tag{8}$$

$$\omega^2 \mu_0 \varepsilon_0 n^2 E_y + \frac{\partial^2 E_y}{\partial x^2} + \frac{\partial^2 E_y}{\partial y^2} + \frac{\partial^2 E_y}{\partial z^2} - j\frac{\delta}{n^2}\left(\frac{\partial^2 E_x}{\partial y \partial z} - \frac{\partial^2 E_z}{\partial x \partial y}\right) = 0, \tag{9}$$

$$\omega^2\mu_0\varepsilon_0\left(-j\delta E_x + n^2 E_z\right) + \frac{\partial^2 E_z}{\partial x^2} + \frac{\partial^2 E_z}{\partial y^2} + \frac{\partial^2 E_z}{\partial z^2} - j\frac{\delta}{n^2}\left(\frac{\partial^2 E_x}{\partial z^2} - \frac{\partial^2 E_z}{\partial x \partial z}\right) = 0. \quad (10)$$

The spatial derivatives in Eqs. (8)–(10) are now calculated by considering Eq. (5):

$$\left(\omega^2\mu_0\varepsilon_0 n^2 - |\gamma|^2 - j\frac{\delta}{n^2}\gamma_x\gamma_z\right)E_x + j\delta\left(\omega^2\mu_0\varepsilon_0 - \frac{1}{n^2}\gamma_x^2\right)E_z = 0 \quad (11)$$

$$\left(\omega^2\mu_0\varepsilon_0 n^2 - |\gamma|^2\right)E_y + j\frac{\delta}{n^2}\left(\gamma_y\gamma_z E_x - \gamma_x\gamma_y E_z\right) = 0, \quad (12)$$

$$-j\delta\left(\omega^2\mu_0\varepsilon_0 - \frac{1}{n^2}\gamma_z^2\right)E_x + \left(\omega^2\mu_0\varepsilon_0 n^2 - |\gamma|^2 - j\frac{\delta}{n^2}\gamma_x\gamma_z\right)E_z = 0, \quad (13)$$

where $|\gamma| = \sqrt{\gamma_x^2 + \gamma_y^2 + \gamma_z^2}$.

2.1.1 TEM wave with electric field vector parallel to H_{DC}

By observing Eqs. (11–13), we note that **when the electric field of the electromagnetic wave is polarized along the y-axis and is parallel to H_{DC}**, so that $E_x = E_z = 0$, the magneto-optical constant δ related to H_{DC} will have no effect on the propagation characteristics of the wave. In this case, from Eq. (12), the propagation constant modulus would be

$$|\gamma| = n\omega\sqrt{\mu_0\varepsilon_0}, \quad (14)$$

which is the same expression for a traveling wave in an isotropic material. Note that when the electric field is polarized along the y-axis, the wave is traveling in the plane xz, so that $\gamma_y = 0$.

2.1.2 The general expression for the propagation constant

In a general case, by solving the system formed by Eqs. (11) and (13), we obtain the following equation

$$\left(\omega^2\mu_0\varepsilon_0 n^2 - |\gamma|^2 - j\frac{\delta}{n^2}\gamma_x\gamma_z\right)^2 - \delta^2\left(\omega^2\mu_0\varepsilon_0 - \frac{1}{n^2}\gamma_x^2\right)\left(\omega^2\mu_0\varepsilon_0 - \frac{1}{n^2}\gamma_z^2\right) = 0. \quad (15)$$

Solving Eq. (15) for $|\gamma|$, we obtain:

$$|\gamma| = \sqrt{\omega^2\mu_0\varepsilon_0 n^2 - j\frac{\delta}{n^2}\gamma_x\gamma_z \pm \delta\sqrt{\left(\omega^2\mu_0\varepsilon_0 - \frac{1}{n^2}\gamma_x^2\right)\left(\omega^2\mu_0\varepsilon_0 - \frac{1}{n^2}\gamma_z^2\right)}}. \quad (16)$$

Note that when the MO constant $\delta = 0$, Eq. (16) reduces to Eq. (14).

The parameters γ_x and γ_z are projections of the propagation constant vector along the x and the y-axis, respectively.

2.1.3 TEM wave propagating parallel to H_{DC}

If the TEM wave is propagating along the H_{DC} direction (y-axis), so that $\gamma_x = \gamma_z = 0$, Eq. (16) assumes the simpler form:

$$|\gamma| = \omega\sqrt{\mu_0\varepsilon_0(n^2 \pm \delta)}, \tag{17}$$

and from Eq. (5), the electric field vector becomes

$$\overline{E} = \left(E_{0x}\vec{\mathbf{i}} + E_{0z}\vec{\mathbf{k}}\right)\exp\left[j\left(\omega t - y\omega\sqrt{\mu_0\varepsilon_0(n^2 \pm \delta)}\right)\right]. \tag{18}$$

From Eq. (11), we see that the electric field components are connected by

$$E_{0x} = -j\delta\frac{\omega^2\mu_0\varepsilon_0}{\left(\omega^2\mu_0\varepsilon_0 n^2 - |\gamma|^2\right)}E_{0z}. \tag{19}$$

Substituting Eq. (17) in Eq. (19), we obtain:

$$E_{0x} = \pm jE_{0z}. \tag{20}$$

Therefore, substituting Eq. (20) in Eq. (18), and given that $\pm j = \exp(\pm j\pi/2)$, the electric field components can be written as

$$E_x = E_{0z}\exp\left[j\left(\omega t - y\omega\sqrt{\mu_0\varepsilon_0(n^2 \pm \delta)} \pm \pi/2\right)\right], \tag{21}$$

$$E_z = E_{0z}\exp\left[j\left(\omega t - y\omega\sqrt{\mu_0\varepsilon_0(n^2 \pm \delta)}\right)\right]. \tag{22}$$

Eqs. (21) and (22) represent a circular polarized wave, which can be dismembered into two circular polarized eigenmodes propagating along the y-axis with different propagation constants. If the plus sign (in "±") is adopted for Eqs. (21) and (22), we obtain a counterclockwise (CCW) circular polarized eigenmode. Otherwise, if the minus sign is adopted, we obtain a clockwise (CW) circular polarized eigenmode, as shown in **Figure 2**. From Eq. (17), it is possible to associate an equivalent refractive index to each eigenmode:

$n^+ = \sqrt{n^2 + \delta}$, for the CCW circular polarized eigenmode;
$n^- = \sqrt{n^2 - \delta}$, for the CW circular polarized eigenmode.

A linear polarized wave propagating along the y-axis may be decomposed into two opposite circular polarized waves in the xz plane, as shown in **Figure 2**. Since these eigenmodes propagate with distinct propagation constants, the linear

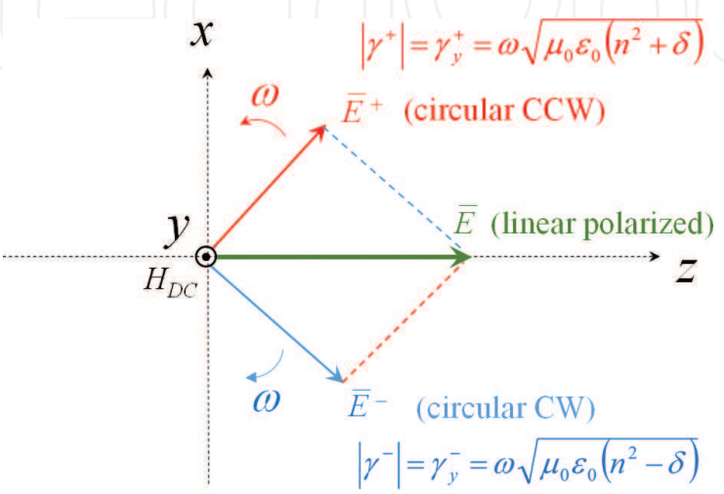

Figure 2.
Decomposition of a linear polarized TEM wave into two circular polarized components. The circular polarized components travel with distinct propagation constants in a MO medium.

polarization will rotate in the *xz* plane as the wave propagates along the *y*-axis, in a phenomenon known as **Faraday rotation**, which is depicted in **Figure 3**.

When the sense of the magnetostatic field H_{DC} is reversed, the magneto-optical constant δ changes its signal, and the values of n^+ and n^- are interchanged, and the sense of rotation of a linear polarized wave in the MO media will change.

The Faraday rotation angle (ϕ_F) may be calculated (in radians) as a function of the propagation distance *y* by

$$\phi_F = \frac{1}{2}(\phi^+ - \phi^-) = \frac{1}{2}\left(n^+\frac{2\pi}{\lambda_0}y - n^-\frac{2\pi}{\lambda_0}y\right) = \frac{\pi}{\lambda_0}\left(\sqrt{n^2+\delta} - \sqrt{n^2-\delta}\right)y, \quad (23)$$

where λ_0 is the optical wavelength in vacuum. The Faraday rotation effect is responsible for a periodic power transfer between the transverse components, in this case, E_x and E_z. This phenomenon in MO materials may be exploited for the design of optical isolators based on Faraday rotation.

When a MO waveguide, with H_{DC} applied along its longitudinal direction, supports degenerate orthogonal quasi TEM modes, the power transfer between these modes will be maximized. **Figure 4** shows a MO rib waveguide [16], where layers 1 and 2 are composed of bismuth yttrium iron garnet (Bi-YIG) grown on top of a gadolinium gallium garnet (GGG) substrate with n_{SR} = 1.94. For the Bi-YIG layers, the relative permittivity tensor has the form of Eq. (2), with $\delta = 2.4 \times 10^{-4}$,

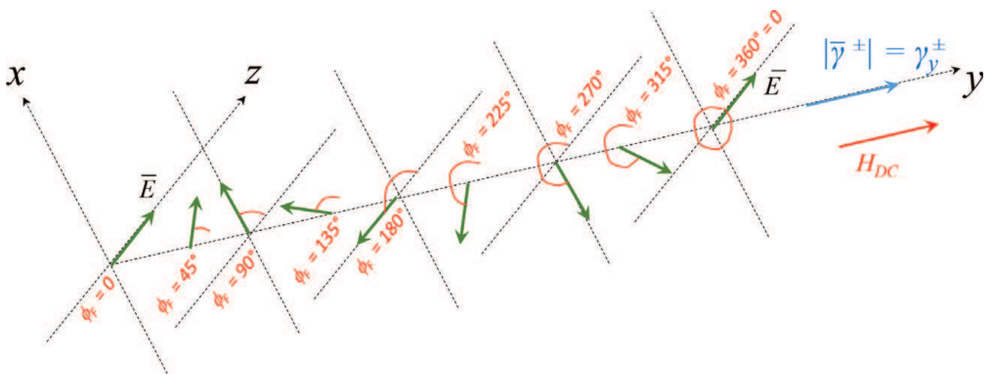

Figure 3.
Faraday rotation of a linear polarized TEM wave in a MO medium. The propagation direction is parallel to the magnetostatic field H_{DC}.

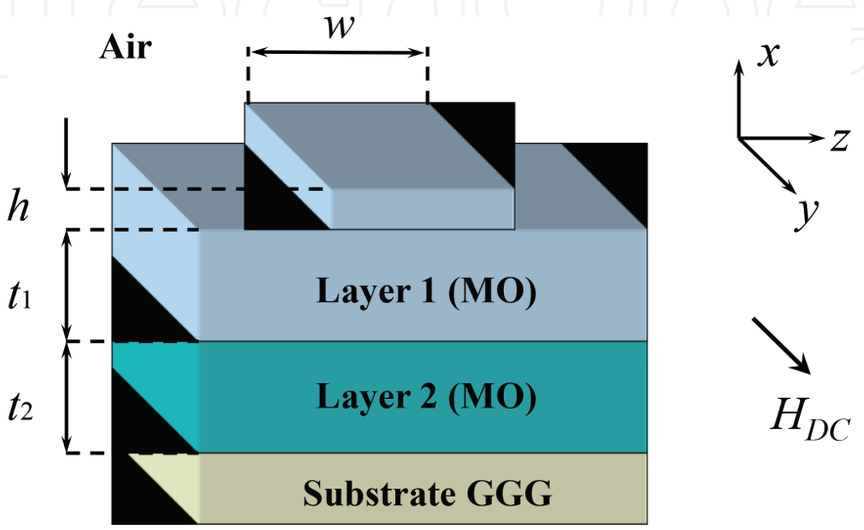

Figure 4.
Magneto-optical rib waveguide.

$n_1 = 2.19$, and $n_2 = 2.18$. The waveguide dimensions are $w = 8$ μm, $h = 0.5$ μm, $t_1 = 3.1$ μm, and $t_2 = 3.4$ μm. The optical wavelength is $\lambda_0 = 1.485$ μm.

Figure 5 shows numerical results for the power transfer between the transverse components along the propagation direction. These results were obtained using a finite difference vectorial beam propagation method (FD-VBPM) [17]. We observe that the length for maximum energy transfer is around 6800 μm. In practice, as observed in [16], the device length must be set at half that length (~3400 μm) so that a 45° rotation is achieved at the output port. Therefore, if a reflection occurs at this point, the reflected field will complete a 90° rotation at the input port, which can then be blocked with a polarizer without affecting the input field, so that an optical isolator is obtained.

In Eq. (23), by adopting $\delta = 2.4 \times 10^{-4}$, $n = n_1 = 2.19$, $\lambda_0 = 1.485$ μm, and $\phi_F = \pi/4$ (45°), we obtain $y = 3388$ μm, which is a propagation length that converges with the FD-VBPM result.

2.1.4 TEM wave propagating along the diagonal of an imaginary cube

Before finishing this section, let us consider another particular case of propagation direction—suppose, in **Figure 1**, that $\gamma_x = \gamma_y = \gamma_z = \gamma_u$, with $\gamma_u \neq 0$. **This case corresponds to a TEM wave propagating along the diagonal of an imaginary cube, adjacent to the Cartesian axes**. From Eq. (16), we obtain:

$$|\gamma| = \sqrt{\omega^2\mu_0\varepsilon_0 n^2 - j\frac{\delta}{n^2}\gamma_u^2 \pm \delta\left(\omega^2\mu_0\varepsilon_0 - \frac{1}{n^2}\gamma_u^2\right)}. \tag{24}$$

From the relation $|\gamma| = \sqrt{\gamma_x^2 + \gamma_y^2 + \gamma_z^2}$ we can also obtain:

$$|\gamma| = \gamma_u\sqrt{3}. \tag{25}$$

Equaling Eqs. (24)–(25) and solving for γ_u result in

$$\gamma_u = \omega\sqrt{\frac{\mu_0\varepsilon_0(n^2 \pm \delta)}{3 \pm \frac{\delta}{n^2} + j\frac{\delta}{n^2}}}. \tag{26}$$

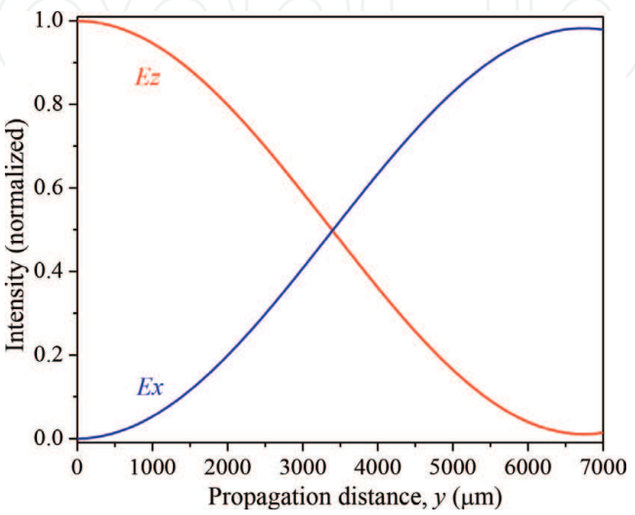

Figure 5.
Normalized intensity evolution of the transverse field components along the propagation direction (y-axis) of the MO waveguide.

Substituting Eq. (26) in Eq. (25), we obtain the propagation constant:

$$|\gamma| = \omega\sqrt{\frac{\mu_0\varepsilon_0(n^2 \pm \delta)}{1 \pm \frac{\delta}{3n^2} + j\frac{\delta}{3n^2}}}. \tag{27}$$

The corresponding electric field vector can be retrieved by substituting the results of Eqs. (26)–(27) in Eq. (11) to obtain

$$E_x = \pm jE_z. \tag{28}$$

However, for the considered propagation direction, the E_y component is not zero. From Eq. (12) we obtain:

$$E_y = -\frac{n^2 \pm \delta + j3(\delta \pm n^2)}{5n^2}E_z. \tag{29}$$

By using the results of Eqs. (26)–(29) in Eq. (5), we can express the electric field vector for this particular case by

$$\overline{E} = \left(\pm j\,\vec{\mathbf{i}} - \frac{n^2 \pm \delta + j3(\delta \pm n^2)}{5n^2}\,\vec{\mathbf{j}} + \vec{\mathbf{k}}\right)E_{0z}\exp\left[j\left(\omega t - \omega\sqrt{\frac{\mu_0\varepsilon_0(n^2 \pm \delta)}{3 \pm \frac{\delta}{n^2} + j\frac{\delta}{n^2}}}(x + y + z)\right)\right], \tag{30}$$

where **i**, **j**, and **k** are the unit vectors along the x-, y-, and z-axis, respectively.

As in the previous case of propagation, Eq. (30) provides two eigenmodes for TEM propagation. From Eq. (28) we can observe that, when projected in the *xz* plane, the electric field vector of each eigenmode is circular polarized. The combination of these eigenmodes will result in a wave with linear polarization progressively rotated as it propagates. The E_y component has the role of projecting the Faraday rotation to the plane perpendicular to the propagation direction (the diagonal of the cube), since the wave is TEM regarding this propagation direction. **Figure 6** shows a simulation of the TEM wave eigenmodes along the diagonal of an imaginary cube.

The simulations presented in **Figure 6** were performed for f = 193.4145 THz, n = 2, and δ = 0.2. Note that both eigenmodes present losses as they propagate. This is due the complex characteristic of the propagation constant expressed by Eq. (27), where the imaginary part depends on the magneto-optical constant δ. It was observed that increasing δ enhances the Faraday rotation but also increases the losses for diagonal propagation.

Equivalent refractive indexes for the circular polarized eigenmodes can be obtained from Eq. (27), which leads to the following equation to compute the Faraday rotation for diagonal propagation:

$$\phi_F = \frac{\pi}{\lambda_0}\mathrm{Re}\left(\sqrt{\frac{n^2 + \delta}{1 + \frac{\delta}{3n^2} + j\frac{\delta}{3n^2}}} - \sqrt{\frac{n^2 - \delta}{1 - \frac{\delta}{3n^2} + j\frac{\delta}{3n^2}}}\right)d, \tag{31}$$

where d is the propagation distance along the diagonal.

For n = 2, δ = 0.2, and λ_0 = 1.55 μm, we obtain ϕ_F/d = 0.27046 rads/μm. Comparing with the case for propagation along the y-axis (parallel to H_{DC}), by using Eq. (23), we obtain ϕ_F/y = 0.40549 rads/μm. These results show that we can obtain a better Faraday rotation when the propagation direction is aligned with the magnetostatic field, when considering TEM waves.

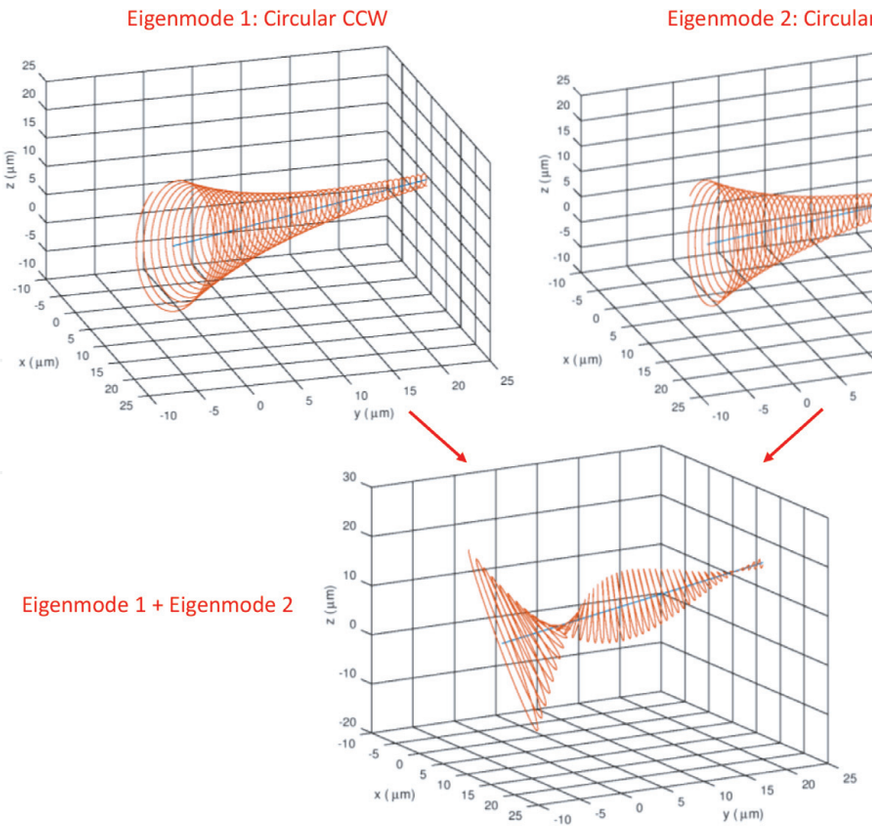

Figure 6.
TEM eigenmodes for diagonal propagation where $\gamma_x = \gamma_y = \gamma_z$. The trajectory of the electric field vector is represented by red lines.

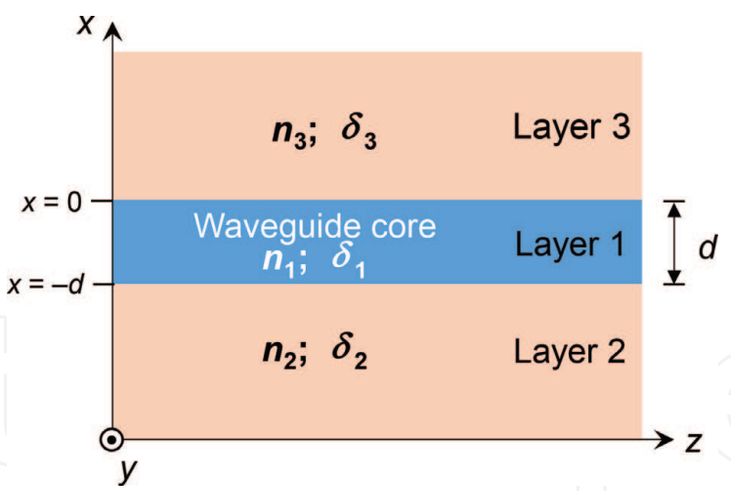

Figure 7.
Longitudinal section of a planar MO waveguide.

2.2 TM mode in a planar magneto-optical waveguide

Figure 7 presents a planar MO waveguide, which is composed by three MO layers. The magnetostatic field H_{DC} is applied along the y-axis. The propagation direction is now the z-axis. The planar waveguide supports transversal electric, TE, modes (H_x, E_y, H_z components) and transversal magnetic, TM, modes (E_x, H_y, E_z components). As discussed in Section 2.1.1, if H_{DC} is parallel to the electric field vector of the wave, then MO constant δ does not affect the propagation characteristics of the mode. Therefore, for the TE modes, no MO effect will be observed. For TM modes, however, the electric field components are perpendicular to H_{DC}, and

nonreciprocal propagation characteristics will take place. In this section, mathematical expressions to calculate the propagation constants for TM modes in a MO planar waveguide will be derived. For the occurrence of guided modes in the structure shown in **Figure 7**, $n_1 > n_2$ and $n_1 > n_3$.

Defining $\overline{\overline{\xi}}$ as the inverse of the electric permittivity tensor of Eq. (2), we have:

$$\overline{\overline{\xi}} = \overline{\overline{\varepsilon}}_r^{-1} = \begin{bmatrix} \frac{n^2}{n^4-\delta^2} & 0 & -\frac{j\delta}{n^4-\delta^2} \\ 0 & \frac{n^2}{n^4-\delta^2} & 0 \\ \frac{j\delta}{n^4-\delta^2} & 0 & \frac{n^2}{n^4-\delta^2} \end{bmatrix} = \begin{bmatrix} \xi_{xx} & 0 & -\xi_{zx} \\ 0 & \xi_{yy} & 0 \\ \xi_{zx} & 0 & \xi_{zz} \end{bmatrix}. \tag{32}$$

From Maxwell's equations at the frequency domain, considering TM modes (E_x, H_y, E_z components) and no field spatial variations along the y-axis, we obtain:

$$j\omega\mu H_y = j\beta E_x + \frac{\partial E_z}{\partial x}, \tag{33}$$

$$E_x = \frac{1}{\varepsilon_0}\left(\xi_{xx}\frac{\beta}{\omega}H_y + j\frac{\xi_{zx}}{\omega}\frac{\partial H_y}{\partial x}\right), \tag{34}$$

$$E_z = \frac{1}{\varepsilon_0}\left(\xi_{zx}\frac{\beta}{\omega}H_y - j\frac{\xi_{zz}}{\omega}\frac{\partial H_y}{\partial x}\right), \tag{35}$$

where β is the propagation constant of the guided TM mode in radians per meter.

Substituting Eqs. (34)–(35) in Eq. (33), we obtain the following wave equation for nonreciprocal media in terms of the H_y component:

$$\frac{\partial^2 H_y}{\partial x^2} + \left(\frac{k_0^2 - \xi_{xx}\beta^2}{\xi_{zz}}\right)H_y = 0, \tag{36}$$

where $k_0 = \omega\sqrt{\mu\varepsilon_0}$.

The solution for H_y is expressed for each waveguide layer as.

$$H_y = C\exp(-\zeta x), \text{ for } x \geq 0. \tag{37}$$

$$H_y = C\cos(\kappa x) + D\,\mathrm{sen}(\kappa x), \text{ for–d} \leq x \leq 0. \tag{38}$$

$$H_y = [C\cos(\kappa d) - D\,\mathrm{sen}(\kappa d)]\exp[\gamma(x+d)], \text{ for } x \leq -\mathrm{d}. \tag{39}$$

The solution for the component E_z at each layer is obtained by substituting the corresponding solution for H_y in Eq. (35), resulting in.

$$E_z = \frac{C}{\omega\varepsilon_0}\left(\xi_{zx}^{(3)}\beta + j\zeta\xi_{zz}^{(3)}\right)\exp(-\zeta x), \text{ for } x \geq 0. \tag{40}$$

$$E_z = \frac{1}{\omega\varepsilon_0}\left\{C\left[\xi_{zx}^{(1)}\beta\cos(\kappa x) + j\kappa\xi_{zz}^{(1)}\mathrm{sen}(\kappa x)\right] + D\left[\xi_{zx}^{(1)}\beta\mathrm{sen}(\kappa x) - j\kappa\xi_{zz}^{(1)}\cos(\kappa x)\right]\right\}, \text{ for–d} \leq x \leq 0. \tag{41}$$

$$E_z = \frac{C\cos(\kappa d) - D\mathrm{sen}(\kappa d)}{\omega\varepsilon_0}\left(\xi_{zx}^{(2)}\beta - j\gamma\xi_{zz}^{(2)}\right)\exp[\gamma(x+d)], \text{ for } x \leq -\mathrm{d}. \tag{42}$$

The superscripts between parentheses on the inverse permittivity tensor elements identify the corresponding waveguide layer, as specified in **Figure 7**. The continuity of E_z at $x = 0$ and at $x = -d$ leads to the following system:

$$C\left[\left(\xi_{zx}^{(3)}-\xi_{zx}^{(1)}\right)\beta+j\zeta\xi_{zz}^{(3)}\right]+D\left(j\kappa\xi_{zz}^{(1)}\right)=0, \tag{43}$$

$$\begin{aligned}&C\left\{\left[\left(\xi_{zx}^{(1)}-\xi_{zx}^{(2)}\right)\beta+j\gamma\xi_{zz}^{(2)}\right]\cos(\kappa d)-j\kappa\xi_{zz}^{(1)}\,sen(\kappa d)\right\}\\&+D\left\{\left[\left(\xi_{zx}^{(2)}-\xi_{zx}^{(1)}\right)\beta-j\gamma\xi_{zz}^{(2)}\right]\mathrm{sen}(\kappa d)-j\kappa\xi_{zz}^{(1)}\cos(\kappa d)\right\}=0.\end{aligned} \tag{44}$$

After solving this system formed by Eqs. (43)–(44), we obtain:

$$\tan(\kappa d)=\frac{\kappa\xi_{zz}^{(1)}\left[\zeta\xi_{zz}^{(3)}+\gamma\xi_{zz}^{(2)}-j\left(\xi_{zx}^{(3)}-\xi_{zx}^{(2)}\right)\beta\right]}{\left(\kappa\xi_{zz}^{(1)}\right)^2-\left[\left(\xi_{zx}^{(3)}-\xi_{zx}^{(1)}\right)\beta+j\zeta\xi_{zz}^{(3)}\right]\left[\left(\xi_{zx}^{(2)}-\xi_{zx}^{(1)}\right)\beta-j\gamma\xi_{zz}^{(2)}\right]}. \tag{45}$$

The constants ζ, κ, and γ can be determined by substituting Eq. (37), Eq. (38), or Eq. (39), respectively, in Eq. (36), resulting in

$$\zeta=\sqrt{\frac{\xi_{xx}^{(3)}\beta^2-k_0^2}{\xi_{zz}^{(3)}}}, \tag{46}$$

$$\kappa=\sqrt{\frac{k_0^2-\xi_{xx}^{(1)}\beta^2}{\xi_{zz}^{(1)}}}, \tag{47}$$

$$\gamma=\sqrt{\frac{\xi_{xx}^{(2)}\beta^2-k_0^2}{\xi_{zz}^{(2)}}}, \tag{48}$$

where $k_0 = 2\pi/\lambda_0$, and λ_0 is the optical wavelength.

From the roots of Eq. (45) for β, the dispersion curve for TM modes in MO waveguides can be retrieved. Assuming that $n_1 = 2.26$, $n_2 = 2.0$, $n_3 = 2.23$, $d = 1$ μm, and only the layer 3 is magneto-optical with $\delta = 0.019$, the dispersion curve for the fundamental and a superior TM mode is shown in **Figure 8**. We observe that the effective index profile changes when the propagation direction is reversed, which opens the possibility to the design of nonreciprocal devices. This phenomenon is known as *nonreciprocal phase shift*. If the magnetostatic field is not applied ($\delta = 0$), the effective index profile becomes reciprocal and converges to the dashed line

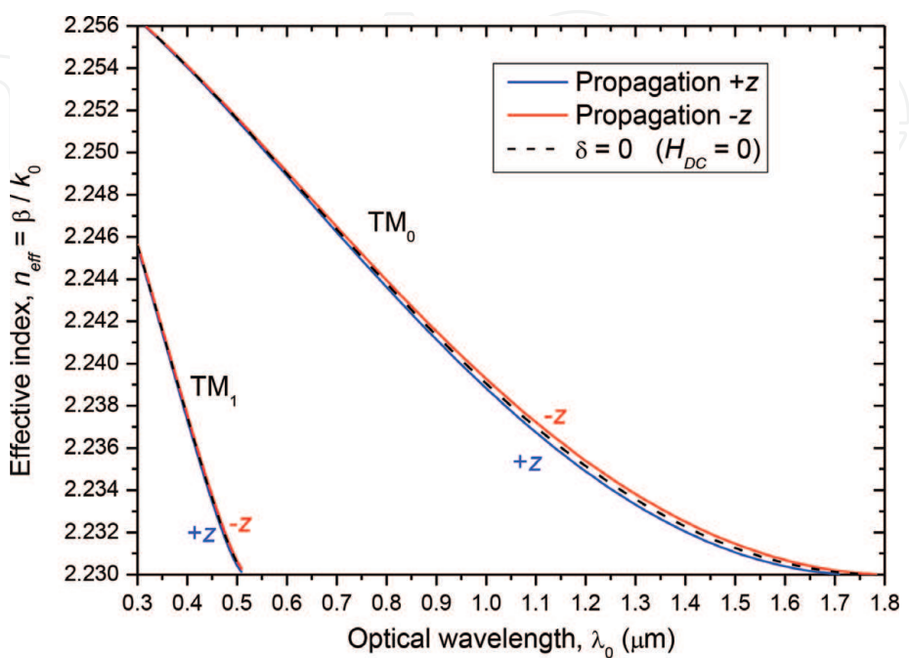

Figure 8.
Dispersion curves of the fundamental TM_0 mode and the superior TM_1 mode.

shown in **Figure 8**. The TM modes reach cutoff for optical wavelengths at which the effective index reaches the minimum value of 2.23. For greater optical wavelengths, the mode becomes irradiated and escapes through layer 3.

Figure 9 shows the transversal distributions of the H_y component at two distinct optical wavelengths. For this waveguide design, λ_0 = 1.55 μm is near cutoff, and the mode is highly distributed in the MO layer, which increases the nonreciprocal phase shift. Note from **Figure 8** that the difference between the effective indexes of the counter propagating TM modes are greater for optical wavelengths near cutoff, but as the wavelengths decreases, the mode becomes more confined at the waveguide core, and its interaction with the MO layer decreases, resulting in a decrease of the nonreciprocal phase shift effect, considering this waveguide configuration.

2.3 TM mode in a planar magneto-optical directional coupler

Now let us consider a five-layered MO planar structure as shown in **Figure 10**.

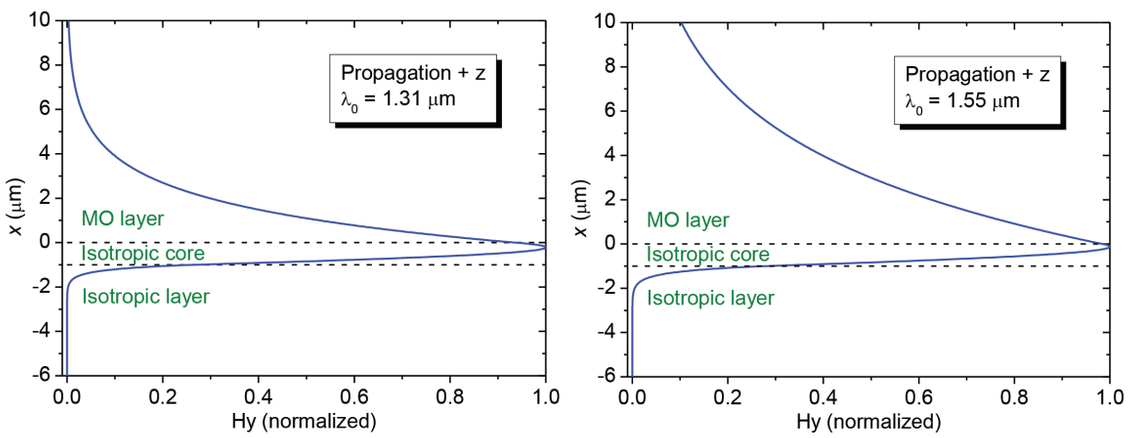

Figure 9.
Transversal distribution of the H_y *component of the fundamental* TM_o *mode at* λ_o = 1.31 μm *and at* λ_o = 1.55 μm.

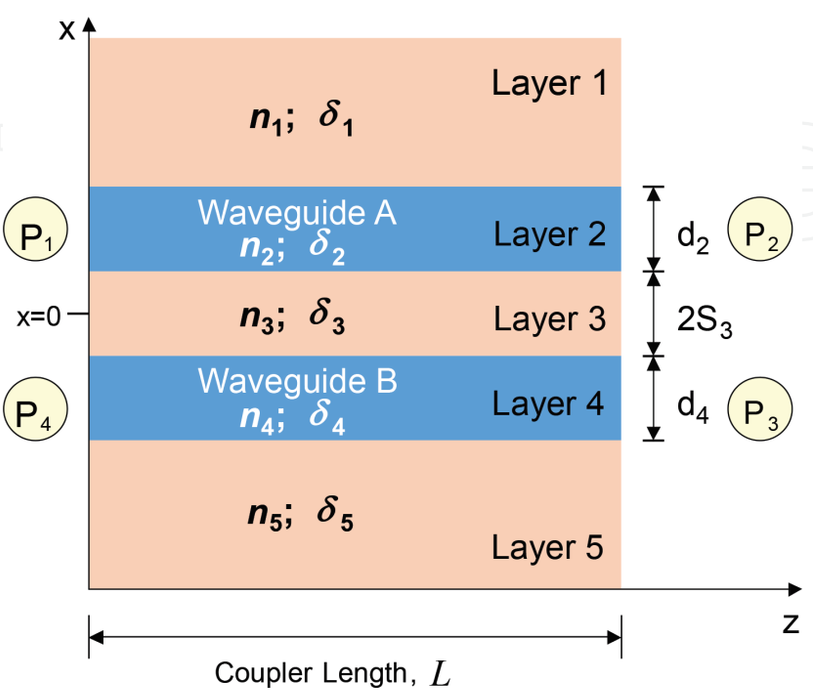

Figure 10.
Longitudinal section of the five-layered MO planar structure.

The solutions for Eq. (36) in each layer, making use of the proper radiation conditions, are [18]

$$H_y = A_1 \exp\left[-\gamma_1(x - S_3 - d_2)\right], \text{ for } x \geq S_3 + d_2,$$
$$H_y = A_2 \cos\left[\kappa_2(x - S_3 - d_2/2)\right] + A_3 \sin\left[\kappa_2(x - S_3 - d_2/2)\right] \text{ for } S_3 \leq x \leq S_3 + d_2,$$
$$H_y = A_4 \exp\left(-\gamma_3 x\right) + A_5 \exp\left(\gamma_3 x\right), \text{ for } -S_3 \leq x \leq S_3,$$
$$H_y = A_6 \cos\left[\kappa_4(x + S_3 + d_4/2)\right] + A_7 \sin\left[\kappa_4(x + S_3 + d_4/2)\right], \text{ for } -S_3 - d_4 \leq x \leq -S_3,$$
$$H_y = A_8 \exp\left[\gamma_5(x + S_3 + d_4)\right], \text{ for } x \leq -S_3 - d_4,$$

where A_1 through A_8 are constants to be determined, κ_i and γ_j are given by.

$$\kappa_i = \sqrt{\frac{k_0^2 - \xi_{xx}^{(i)}\beta^2}{\xi_{zz}^{(i)}}}, i = 2, 4, \tag{49}$$

$$\gamma_j = \sqrt{\frac{\xi_{xx}^{(j)}\beta^2 - k_0^2}{\xi_{zz}^{(j)}}}, j = 1, 3, 5, \tag{50}$$

where $k_0 = 2\pi/\lambda_0$, and λ_0 is the optical wavelength.

The electric field components E_x and E_z can be directly obtained with Eq. (34) and Eq. (35), respectively. Applying the boundary conditions for the tangential components H_y and E_z, one obtains a system of eight equations and eight unknowns, which can be conveniently written in matrix form as follows:

$$[M(\beta)]\mathbf{A} = \mathbf{0}. \tag{51}$$

Here, $[M(\beta)]$ is an 8×8 matrix that depends on the unknown longitudinal propagation constant β and $\mathbf{A} = [A_1\ A_2\ \ldots\ A_8]^{\mathrm{T}}$. The propagation constant can be easily found by solving the equation $Det([M(\beta)]) = 0$. The nonzero elements of the matrix $[M(\beta)]$ are listed below:

$$M_{11} = 1; M_{12} = -\cos\left(\kappa_2 d_2/2\right); M_{13} = -\sin\left(\kappa_2 d_2/2\right);$$
$$M_{21} = -j\xi_{zx}^{(1)}\beta + \gamma_1\xi_{zz}^{(1)}; M_{22} = j\xi_{zx}^{(2)}\beta\cos\left(\kappa_2 d_2/2\right) - \kappa_2\xi_{zz}^{(2)}\sin\left(\kappa_2 d_2/2\right);$$
$$M_{23} = -j\xi_{zx}^{(2)}\beta\sin\left(k_2 d_2/2\right) + k_2\xi_{zz}^{(2)}\cos\left(k_2 d_2/2\right);$$
$$M_{32} = \cos\left(\kappa_2 d_2/2\right); M_{33} = -\sin\left(\kappa_2 d_2/2\right); M_{34} = -\exp\left(-\gamma_3 S_3\right); M_{35} = -\exp\left(\gamma_3 S_3\right);$$
$$M_{42} = -j\xi_{zx}^{(2)}\beta\cos\left(\kappa_2 d_2/2\right) - \kappa_2\xi_{zz}^{(2)}\sin\left(\kappa_2 d_2/2\right);$$
$$M_{43} = j\xi_{zx}^{(2)}\beta\sin\left(\kappa_2 d_2/2\right) - \kappa_2\xi_{zz}^{(2)}\cos\left(\kappa_2 d_2/2\right);$$
$$M_{44} = \left(j\xi_{zx}^{(3)}\beta - \xi_{zz}^{(3)}\gamma_3\right)\exp\left(-\gamma_3 S_3\right); M_{45} = \left(j\xi_{zx}^{(3)}\beta + \xi_{zz}^{(3)}\gamma_3\right)\exp\left(\gamma_3 S_3\right);$$
$$M_{54} = \exp\left[\gamma_3 S_3\right]; M_{55} = \exp\left[-\gamma_3 S_3\right]; M_{56} = -\cos\left(\kappa_4 d_4/2\right); M_{57} = -\sin\left(\kappa_4 d_4/2\right);$$
$$M_{64} = -\left(j\xi_{zx}^{(3)}\beta + \xi_{zz}^{(3)}\gamma_3\right)\exp\left[\gamma_3 S_3\right]; M_{65} = -\left(j\xi_{zx}^{(3)}\beta + \xi_{zz}^{(3)}\gamma_3\right)\exp\left[-\gamma_3 S_3\right];$$
$$M_{66} = j\xi_{zx}^{(4)}\beta\cos\left(\kappa_4 d_4/2\right) - \xi_{zz}^{(4)}\kappa_4\sin\left(\kappa_4 d_4/2\right);$$
$$M_{67} = j\xi_{zx}^{(4)}\beta\sin\left(\kappa_4 d_4/2\right) + \xi_{zz}^{(4)}\kappa_4\cos\left(\kappa_4 d_4/2\right);$$
$$M_{76} = \cos\left(\kappa_4 d_4/2\right); M_{77} = -\sin\left(\kappa_4 d_4/2\right); M_{78} = -1;$$
$$M_{86} = -j\xi_{zx}^{(4)}\beta\cos\left(\kappa_4 d_4/2\right) - \xi_{zz}^{(4)}\kappa_4\sin\left(\kappa_4 d_4/2\right);$$
$$M_{87} = j\xi_{zx}^{(4)}\beta\sin\left(\kappa_4 d_4/2\right) - \xi_{zz}^{(4)}\kappa_4\cos\left(\kappa_4 d_4/2\right);$$
$$M_{88} = j\xi_{zx}^{(5)}\beta + \xi_{zz}^{(5)}\gamma_5;$$

As an example, **Table 1** shows the material parameters and layer thicknesses for each layer. Layers 1 and 5 are unbounded, and their thicknesses are theoretically infinite for the analytical model. The optical wavelength is λ_0 = 1.55 μm.

Figure 11 shows a plot of guided supermodes that occurs in the planar structure for forward propagation (along $+z$). The guided propagation along the five-layered structure, as well the periodical energy exchange of light between the two waveguides, can be expressed as a linear combination of these supermodes. The coupling length for the structure is given by $L_\pi = \pi/|\beta_1 - \beta_2|$, where β_1 and β_2 are the propagation constants of the supermodes obtained from the roots of $Det([M(\beta)]) = 0$. The computed coupling length, which refers to the propagation along the $+z$ axis, is $L_\pi^+ = 1389.84\ \mu m$.

Figure 12 shows the plot of the supermodes, now considering backward propagation of the TM mode (along $-z$). The computed coupling length, which refers to the backward propagation along the z-axis, is $L_\pi^- = 689\,\mu m$.

Layer	Parameters		
	n	δ	Thickness (μm)
1	2.23	−0.019	∞
2	2.26	0	1.20
3	2.00	0	0.75
4	2.26	0	1.23
5	2.23	−0.019	∞

Table 1.
Material and geometric parameters of the MO directional coupler.

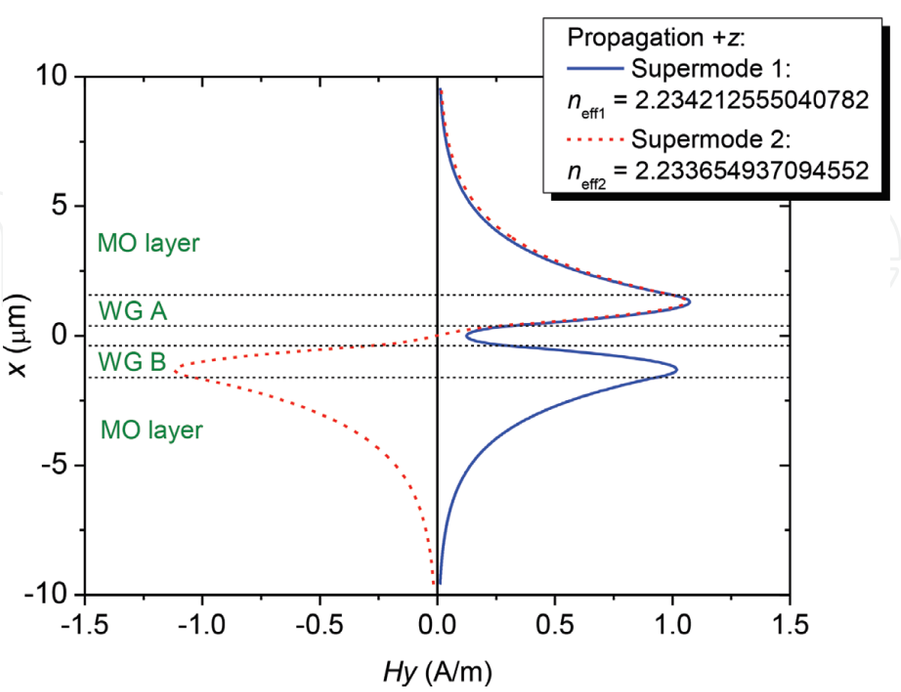

Figure 11.
Transversal distribution of the supermodes (H_y component) for forward propagation ($+z$).

Considering both propagation senses, when the condition $L = L_{\pi}^{+} = 2L_{\pi}^{-}$ for the length of the directional coupler is achieved, we obtain an optical isolator calibrated for the given optical wavelength. The operation of the optical isolator is depicted in **Figure 13**. If an optical source is placed at the port 1 of the waveguide A, all optical power will be coupled into port 3 of the waveguide B, if the length of the directional coupler is $L = L_{\pi}^{+}$. If some light is reflected at port 3, since $L = 2L_{\pi}^{-}$, all optical power is directed to the port 4. Therefore, the optical source at port 1 becomes isolated from the reflected light. **Figures 14**, **15** show simulations of the forward and backward optical propagation in the MO directional coupler via a propagation projection of a linear combination of the corresponding supermodes.

The MO directional coupler of **Figure 10** also acts as an optical circulator, considering the following sequence of input and output ports: 1 to 3; 3 to 4; 4 to 2; and 2 to 1.

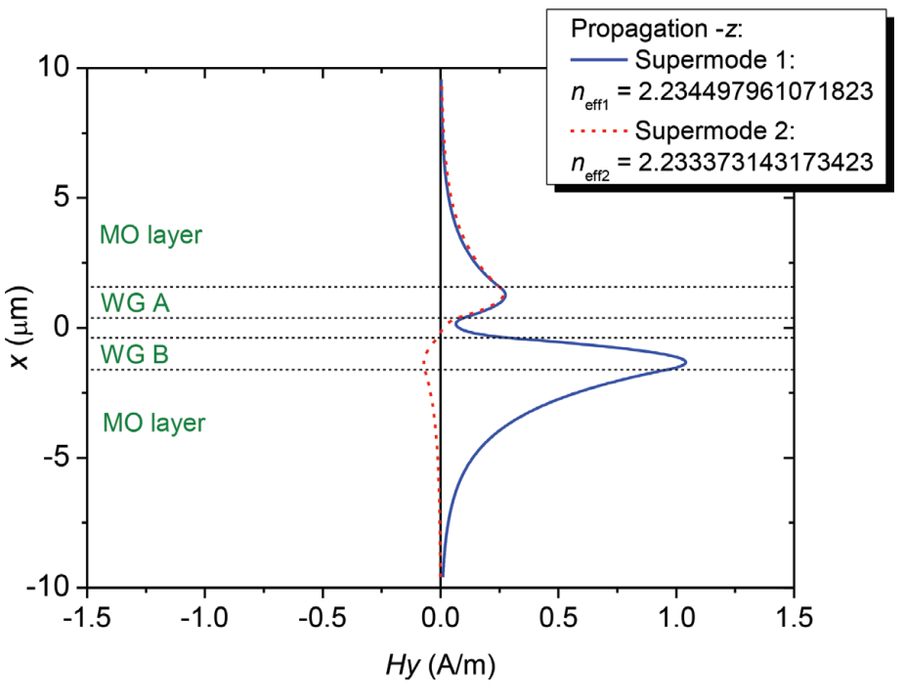

Figure 12.
Transversal distribution of the supermodes (H_y component) for backward propagation (−z).

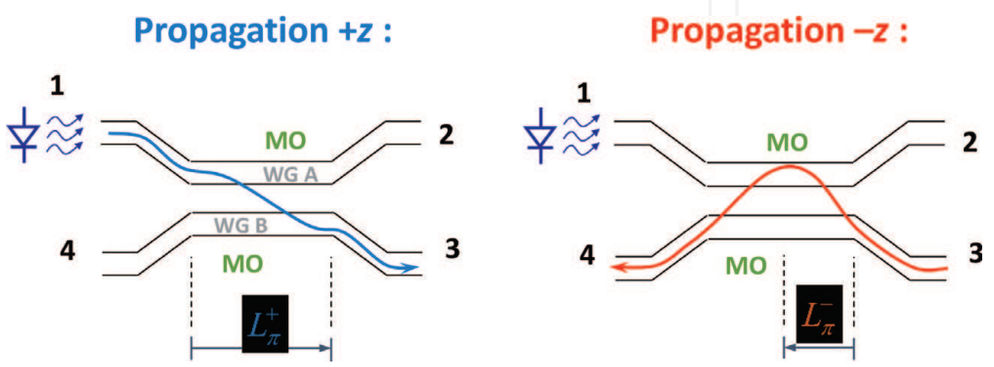

Figure 13.
Operation of an optical isolator based on nonreciprocal phase shift.

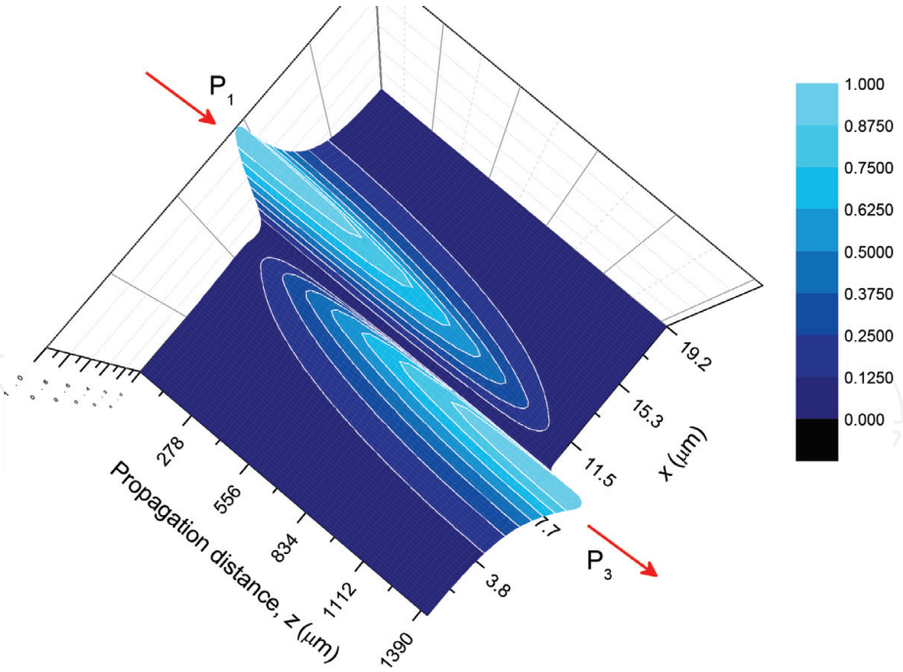

Figure 14.
Forward propagation simulation of the TM mode component H_y *excited at port 1 (*P_1*) of the five-layered structure. The light exits through port 3 (*P_3*). The starting transversal* H_y *field was supermode 1 plus supermode 2 of* ***Figure 11****.*

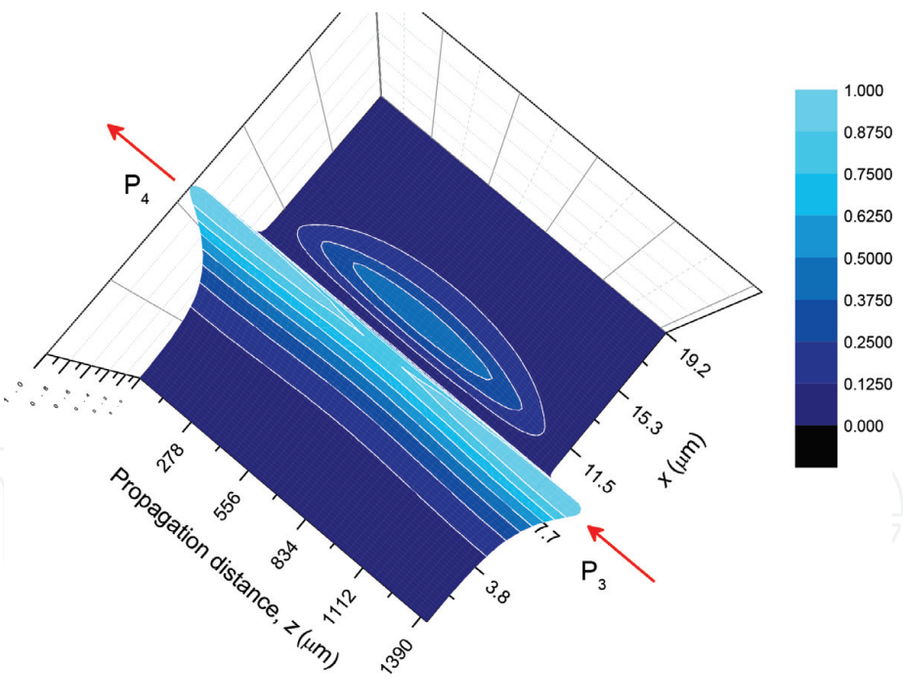

Figure 15.
Backward propagation simulation of the TM mode component H_y *excited at port 3 (*P_3*) of the five-layered structure. The light exits through port 4 (*P_4*). The starting transversal* H_y *field was supermode 1 minus supermode 2 of* ***Figure 12****.*

3. Conclusions

The propagation characteristics of optical waves in magneto-optical media and in planar waveguides with three and five MO layers were exposed. The effects of Faraday rotation and nonreciprocal phase shift were discussed with mathematical

background to support the analyses. The propagation of TEM waves in unbounded MO media was discussed, where it was shown that the Faraday rotation is maximized when the propagation occurs in the same direction of the applied magnetostatic field. It was also mathematically shown that if there is no such alignment, losses may be added to the wave propagation. A planar MO waveguide and a directional coupler were also analyzed in the context of their nonreciprocity. For these structures, nonreciprocity is observed for TM-guided modes. The theoretical analyses confirm that magneto-optical materials have great potential to be employed on the design of nonreciprocal optical devices, such as isolators and circulators.

IntechOpen

IntechOpen

Author details

Licinius Dimitri Sá de Alcantara
Cyberspatial Institute, Federal Rural University of Amazon, Belém, Brazil

*Address all correspondence to: licinius@ufra.edu.br

IntechOpen

© 2018 The Author(s). Licensee IntechOpen. This chapter is distributed under the terms of the Creative Commons Attribution License (http://creativecommons.org/licenses/by/3.0), which permits unrestricted use, distribution, and reproduction in any medium, provided the original work is properly cited. CC BY

References

[1] Antonov V, Harmon B, Yaresko A. Electronic Structure and Magneto-Optical Properties of Solids. Dordrecht: Springer; 2004. 528 p. DOI: 10.1007/1-4020-1906-8

[2] Levy M. The on-chip integration of magnetooptic waveguide isolators. IEEE Journal of Selected Topics in Quantum Electronics. 2002;**8**(6):1300-1306. DOI: 10.1109/JSTQE.2002.806691

[3] Ando K. Waveguide optical isolator: A new design. Applied Optics. 1991; **30**(9):1080-1095. DOI: 10.1364/AO.30.001080

[4] Bahlmann N, Chandrasekhara V, Erdmann A, Gerhardt R, Hertel P, Lehmann R, et al. Improved design of magnetooptic rib waveguides for optical isolators. Journal of Lightwave Technology. 1998;**16**(5):818-823. DOI: 10.1109/50.669010

[5] Li TF, Guo TJ, Cui HX, Yang M, Kang M, Guo QH, et al. Guided modes in magneto-optical waveguides and the role in resonant transmission. Optics Express. 2013;**21**(8):9563-9572. DOI: 10.1364/OE.21.009563

[6] Bolduc M, Taussig AR, Rajamani A, Dionne GF, Ross CA. Magnetism and magnetooptical effects in Ce-Fe oxides. IEEE Transactions on Magnetics. 2006; **42**(10):3093-3095. DOI: 10.1109/TMAG.2006.880514

[7] Fratello VJ, Licht SJ, Brandle CD. Innovative improvements in bismuth doped rare-earth iron garnet Faraday rotators. IEEE Transactions on Magnetics. 1996;**32**(5):4102-4107. DOI: 10.1109/20.539312

[8] Pedroso CB, Munin E, Villaverde AG, Medeiros Neto JA, Aranha N, Barbosa LC. High Verdet constant Ga:S:La:O chalcogenide glasses for magneto-optical devices. Optical Engineering. 1999;**38**(2). DOI: 10.1117/1.602080

[9] Kalandadze L. Influence of implantation on the magneto-optical properties of garnet surface. IEEE Transactions on Magnetics. 2008; **44**(11):3293-3295. DOI: 10.1109/TMAG.2008.2001624

[10] Nomura T, Kishida M, Hayashi N, Ishibashi T. Evaluation of garnet film as magneto-optic transfer readout film. IEEE Transactions on Magnetics. 2011; **47**(8):2081-2086. DOI: 10.1109/TMAG.2011.2123103

[11] Inoue M, Arai K, Fujii T, Abe M. One-dimensional magnetophotonic crystals. Journal of Applied Physics. 1999;**85**(8):5768-5770. DOI: 10.1063/1.370120

[12] Koerdt C, Rikken GL, Petrov EP. Faraday effect of photonic crystals. Applied Physics Letters. 2003;**82**(10): 1538-1540. DOI: 10.1063/1.1558954

[13] Zvezdin AK, Belotelov VI. Magnetooptical properties of two-dimensional photonic crystals. The European Physical Journal B–Condensed Matter and Complex Systems. 2004;**37**: 479-487. DOI: 10.1140/epjb/e2004-00084-2

[14] Haider T. A review of magneto-optic effects and its application. International Journal of Electromagnetics and Applications. 2017;**7**(1):17-24. DOI: 10.5923/j.ijea.20170701.03

[15] Zak J, Moog ER, Liu C, Bader SD. Magneto-optics of multilayers with arbitrary magnetization directions. Physical Review B. 1991;**43**:6423-6429. DOI: 10.1103/PhysRevB.43.6423

[16] Wolfe R, Lieberman R, Fratello V, Scotti R, Kopylov N. Etch-tuned ridged waveguide magneto-optic isolator. Applied Physics Letter. 1990;**56**: 426-428. DOI: 10.1063/1.102778

[17] Alcantara LDS, Teixeira FL, Cesar AC, Borges BH. A new full-vectorial FD-BPM scheme: Application to the analysis of magnetooptic and nonlinear saturable media. Journal of Lightwave Technology. 2005;**23**(8):2579-2585. DOI: 10.1109/JLT.2005.850811

[18] Alcantara LDS, De Francisco CA, Borges BH. Analytical model for magnetooptic five-layered planar waveguides. In: SBMO/IEEE MTT-S International Microwave and Optoelectronics Conference (IMOC'17); 27–30 August 2017; Águas de Lindóia, Brazil. pp. 1-5. DOI: 10.1109/IMOC.2017.8121106